SENSORIMOTOR CONVERGENCE IN VISUAL NAVIGATION AND FLIGHT CONTROL SYSTEMS

J. Sean Humbert [1] **Richard M. Murray**
Michael H. Dickinson

Division of Engineering and Applied Science
California Institute of Technology, Pasadena, CA 91125

Abstract: Insects exhibit unparalleled and incredibly robust flight dynamics in the face of uncertanties. A fundamental principle contributing to this amazing behavior is rapid processing and convergence of visual sensory information to flight motor commands via spatial wide-field integration. Within the control-theoretic framework presented here, a model for wide-field integration of retinal image flow is developed which explains how various image flow kernels correspond to feedback terms that stabilize the different modes of planar flight. It is also demonstrated that the proposed output feedback methodology is sufficient to explain experimentally observed navigational heuristics as the centering and forward speed regulation responses exhibited by honeybees.

Keywords: Navigation Systems, Output Feedback, Control-Oriented Models, Autonomous Mobile Robots.

1. INTRODUCTION

Prevalent in many natural sensory systems is the phenomenon of sensorimotor convergence, where signals from arrays of spatially distributed and differentially tuned sensors converge in number up to several orders of magnitude to motor neurons responsible for controlling locomotive behavior. An excellent example occurs in the processing of retinal image pattern movement (optic flow) by the visuomotor systems of insects, one of nature's more efficient and successful navigating organisms. Insect visual systems encode optic flow by combining motion estimates from arrays of local motion detectors in a way that preserves the spatial layout of the retina. This information is parsed by wide-field motion sensitive interneurons (tangential cells, or LPTCs) in the lobula plate section of the visual ganglia (Figure 1A). The output of these neurons synapse in the motor control centers, creating a sensory processing stage which spatially integrates the optic flow (Frye and Dickinson, 2001). This sensorimotor convergence technique, spatial wide-field integration, is used by insects to extract control-relevant information from optic flow patterns to modulate the kinematics of locomotion and flight.

Since optic flow was first recognized as a critical source of information (Gibson, 1950), there has been considerable interest in adapting this type of sensory system for bio-inspired autonomous navigation. Efforts have focused on utilizing one or more properties of optic flow to provide navigational cues (Barrows *et al.*, 2003). Examples include corridor navigation based on balancing average lateral image velocities on wheeled robots, as well as obstacle avoidance via saccading away from regions with high image velocities or using optic flow based estimates of depth. In a more tra-

[1] Corresponding author: jshumber@cds.caltech.edu

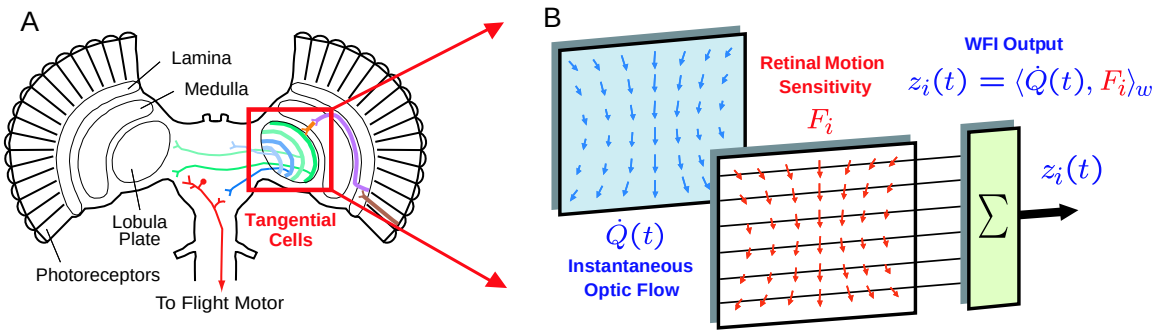

Fig. 1. (A) Visuomotor system of insects. Wide-field retinal motion sensitive interneurons (tangential cells) parse spatially-preserved visual information and transmit it to motor control centers. (B) WFI processing model. Spatial modes of optic flow are extracted by retinal motion sensitivity kernels.

ditional approach, LPTC-based processing models have been investigated as estimators for vehicle kinematic states directly from observed optic flow, as tangential cell sensitivity maps show similarities to flow fields that correspond to egomotion (Krapp and Hengstenberg, 1996).

In this paper we propose a more general role for wide-field sensitive neurons in navigation and flight control as well as a novel methodology for utilizing optic flow in bio-inspired applications. We show how the spatial harmonics of planar optic flow, extracted with motion-pattern sensitive kernels representing LPTCs (Figure 1B), correspond to feedback terms which can be used to stabilize the different navigational modes of flight. The computationally-efficient output feedback methodology presented requires no direct estimation of depth or kinematic states, nor any prior knowledge of the environment.

2. A MODEL FOR WIDE-FIELD INTEGRATION PROCESSING OF IDEAL PLANAR OPTIC FLOW

In the idealized case, optic flow is dependent on rigid body motion (translation and rotation) and on the spatial structure and distribution of objects in the environment. (Koenderink and van Doorn, 1997) provide a thorough derivation of the equations of ideal optic flow based on a three dimensional environment composed of a finite number of rigid fiducial points. For our treatment here we will consider the planar motion case, restricting the rigid body motion to three degrees of freedom (planar translation with single axis rotation). For analysis purposes we will consider the the optic flow to be a function of a continuous angular coordinate γ relative to the body-fixed frame b (Figure 2). Under these assumptions, the instantaneous optic flow on a circular-shaped sensor becomes a 2π-periodic function on the circle S^1 in the angular coordinate γ:

$$\dot{Q}(\gamma) = -\dot{\theta} + \mu(\gamma)\left(\dot{x}_b \sin\gamma - \dot{y}_b \cos\gamma\right), \quad (1)$$

where $\dot{\theta}, \dot{x}_b, \dot{y}_b$ are the kinematics of the body-fixed frame b, and $\mu(\gamma) = 1/r(\gamma)$, where $r(\gamma) : [0, 2\pi] \mapsto (0, \infty)$ is the distance to the nearest obstacle along direction $\boldsymbol{Q}(\gamma) \in S^1$, restricting contact (Figure 2A). The kinematics are assumed to be bounded functions of time, however the spatial structure of the landscape can lead to discontinuities, especially in a cluttered object field. Hence $\mu(\gamma)$ and $\dot{Q}(\gamma)$ can be considered bounded piecewise continuous functions with a finite (countable) number of discontinuities (Figure 2B), effectively restricting them to the space of square-integrable functions $L_2[0, 2\pi] = \left\{ f : [0, 2\pi] \to \mathbb{R} : \int_0^{2\pi} |f(\gamma)|^2 \, d\gamma < \infty \right\}$.

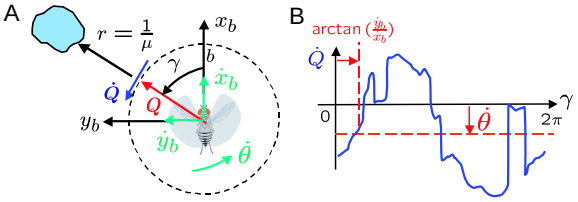

Fig. 2. (A) Body-coordinate definitions (B) Example planar optic flow

For this treatment we will represent the lobula plate tangential cells (or ipsi- and contralateral pairs as may be appropriate) by a weight $F_i(\gamma) \in L_2[0, 2\pi]$, which models their sensitivity to various motion patterns. Weights $F_i(\gamma)$ are essentially a spatially distributed set static gains which are applied to the output at the corresponding local motion detectors at retinal positions γ. Through appropriate choices of $F_i(\gamma)$, we are interested in characterizing the available information relevant for use in closed loop feedback. We expect these weighting functions to be piecewise continuous and square-integrable, hence the restriction to the function space $L_2[0, 2\pi]$. For this initial analysis we will also assume that the optic flow estimation processing block (photoreceptors and local motion detectors) has negligible dynamics, that is wide-field spatial integration (henceforth WFI) can be

modeled in entirety by the transformation W, representing a spatial integration against the optic flow kernel $\dot{Q}(\gamma, t)$, which acts on elements $F_i(\gamma)$ to produce a sensor output signal z_i, hence $W : F_i \in L_2[0, 2\pi] \mapsto z_i \in \mathbb{R}$. The transformation W defined by $z_i = WF_i$ can be represented as a linear functional using the inner product structure available on $L_2[0, 2\pi]$:

$$z_i = \langle \dot{Q}, F_i \rangle_w = \frac{1}{\pi} \int_0^{2\pi} \dot{Q}(\gamma) \cdot F_i(\gamma)\, d\gamma. \qquad (2)$$

The observation equation can be written compactly as $z = WF$, where $z = \{z_i : i = 1, \ldots, m\}$ denotes the set of output measurements generated through WFI sensory processing weights $F = \{F_i : i = 1, \ldots, m\}$. The inner product (2) has been defined with a factor of $1/\pi$ to be compatible with the typical Fourier harmonic component definition so that later notation is simplified.

2.1 Characterization and Interpretation of WFI Sensory Outputs for Planar Optic Flow

We are interested in characterizing the set of all possible sensory outputs available within this model and their dependency on the vehicle motion and the spatial distribution of objects in the environment. Since $L_2[0, 2\pi]$ is a Hilbert space, and more specifically a complete, seperable inner product space, a countably infinite orthonormal basis $\{\phi_n(\gamma)\}$ exists. For fixed t, $\dot{Q}(\gamma, t) \in L_2[0, 2\pi]$, therefore we can expand it in a generalized Fourier series $\dot{Q}(\gamma, t) = \sum_n^\infty \langle \dot{Q}(\gamma, t), \phi_n(\gamma) \rangle\ \phi_n(\gamma)$. If we use trigonometric Fourier series, the orthonormal basis under the inner product (2) is $\Phi = \{1/\sqrt{2}\} \cup \{\cos n\gamma : n = 1, 2, \ldots\} \cup \{\sin n\gamma : n = 1, 2, \ldots\}$, and the expansion becomes $\dot{Q}(\gamma, t) = \frac{a_0(t)}{2} + \sum_{n=1}^\infty a_n(t) \cos n\gamma + b_n(t) \sin n\gamma$, where the time-dependent spatial harmonics of the optic flow are defined as $a_0(t) = \langle \dot{Q}, \cos 0 \rangle_w = \frac{1}{\pi} \int_0^{2\pi} \dot{Q}(\gamma, t)\, d\gamma$, $a_n(t) = \langle \dot{Q}, \cos n\gamma \rangle_w = \frac{1}{\pi} \int_0^{2\pi} \dot{Q}(\gamma, t) \cos n\gamma\ d\gamma$, and $b_n(t) = \langle \dot{Q}, \sin n\gamma \rangle_w = \frac{1}{\pi} \int_0^{2\pi} \dot{Q}(\gamma, t) \sin n\gamma\, d\gamma$. With some manipulations, we can re-write these expressions in terms of the vehicle kinematics $(\dot{x}_b, \dot{y}_b, \dot{\theta})$ and the spatial harmonics $\{A_0, A_k, B_k : k = 1, 2, \ldots\}$ of the nearness function $\mu(\gamma, t)$:

$$\begin{aligned} a_0(t) &= (-\dot{\theta} + \dot{x}_b B_1 - \dot{y}_b A_1)/\sqrt{2} \qquad (3) \\ a_n(t) &= \frac{\dot{x}_b}{2} (-B_{n-1} + B_{n+1}) - \frac{\dot{y}_b}{2} (A_{n-1} + A_{n+1}) \\ b_n(t) &= \frac{\dot{x}_b}{2} (A_{n-1} - A_{n+1}) - \frac{\dot{y}_b}{2} (B_{n-1} + B_{n+1}), \end{aligned}$$

where $\mu(\gamma, t) = \frac{A_0(t)}{2} + \sum_{k=1}^\infty A_k(t) \cos n\gamma + B_k(t) \sin n\gamma$. Now, under the interpretation $W\Phi = \{a_0(t)\} \cup \{a_n(t) : n = 1, 2, \ldots\} \cup \{b_n(t) : n = 1, 2, \ldots\}$, the equations (3) define the action of the linear transformation $W : L_2[0, 2\pi] \mapsto \mathbb{R}$ on a basis Φ for the domain, and as such uniquely characterize the set of all possible wide-field integration sensory outputs.

The relationships in (3) define how WFI outputs depend on vehicle motion $(\dot{x}_b, \dot{y}_b, \dot{\theta})$ and object nearness $\{A_0, A_k, B_k : k = 1, 2, \ldots\}$, however the intuition required to utilize them in closed loop feedback is not readily apparent. The following analysis suggests an output feedback methodology, based on *shaping* the spatial harmonic content of μ, for designing a set of WFI sensory processing weights F to stabilize the different navigational modes of flight. The planar tunnel geometry (Figure 3A), which provides a reasonable approximation to flight between two obstacles, can serve as the motivating example; the nearness function $\mu(\gamma, t)$ can be expressed in closed form if the lateral position y, body frame orientation θ and the tunnel half-width a are known:

$$\mu(\gamma) = \begin{cases} \dfrac{\sin(\gamma + \theta)}{a - y} & 0 \le \gamma + \theta < \pi \\ -\dfrac{\sin(\gamma + \theta)}{a + y} & \pi \le \gamma + \theta < 2\pi \end{cases}. \qquad (4)$$

For the case $y = 0$ and $\theta = 0$, (4) reduces to $|\sin\gamma|\,/a$, which has a Fourier series expansion

$$\left| \frac{\sin\gamma}{a} \right| = \frac{2}{a\pi} - \sum_{k=2,4,6,\ldots}^\infty \frac{4}{a\pi(k^2 - 1)} \cos k\gamma. \qquad (5)$$

Note that the expansion is composed of a DC component and even cosine harmonics $\{A_k : k = 0, 2, 4, \ldots\}$ of decreasing amplitude only. (5) represents the *balanced* or *equilibrium* nearness shape (Figure 3A), as it corresponds to flight along the centerline of a planar tunnel. For small perturbations with respect to a constant-speed centerline reference trajectory, $\dot{x}_b \gg \dot{y}_b$, hence WFI outputs b_n, resulting from weights $\{F_n(\gamma) = \sin n\gamma : n = 1, 3, \ldots\}$, will be predominantly functions of $\{A_k : k = 0, 2, 4, \ldots\}$. These outputs provide an estimate of the average global image angular velocity (optic flow) induced by motion between the walls, as these harmonics should be present in a feedback system that is maintaining the desired μ shape.

If the vehicle is laterally positioned $y = 0$ but not oriented directly along the centerline $\theta \neq 0$, we get a phase shift θ of this function, and using the substitution $\gamma \mapsto \gamma + \theta$ in (5) we obtain the new Fourier series for μ: $\left| \frac{\sin(\gamma+\theta)}{a} \right| = \frac{2}{a\pi} - \sum_{k=2,4,6,\ldots}^\infty \frac{4\cos k\theta}{a\pi(k^2-1)} \cos k\gamma - \sum_{k=2,4,6,\ldots}^\infty \frac{4\sin k\theta}{a\pi(k^2-1)} \sin k\gamma$. This series contains the equilibrium DC component and cosine harmonics $\{A_k : k = 0, 2, 4, \ldots\}$, but now also con-

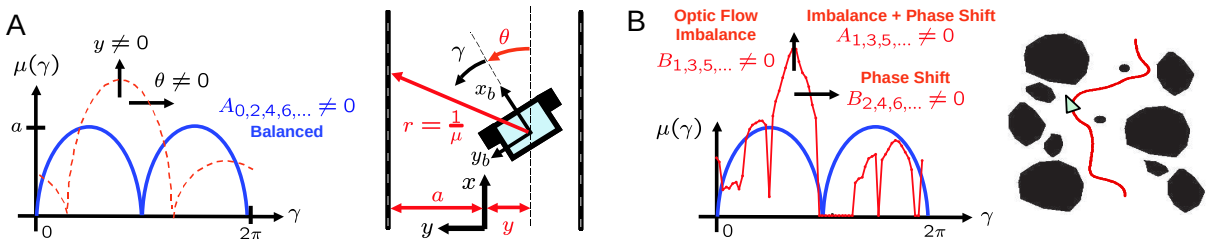

Fig. 3. Connections between WFI outputs and μ. (A) Planar tunnel geometry and lateral/rotational perturbations of μ (B) μ-shaping in environments with higher order spatial structure

tains even sine harmonics $\{B_k : k = 2, 4, 6, \ldots\}$, with amplitudes in proportion to $\sin k\theta$. For small perturbations, outputs a_n generated by weights $\{F_n(\gamma) = \cos n\gamma : n = 1, 3, \ldots\}$ will be functions of $\{B_k : k = 2, 4, 6, \ldots\}$, hence will be responsive to orientation changes with respect to the tunnel centerline. For obstacles with higher order spatial structure, these outputs will reflect rotational alignment with respect to a desired forward flight path between the obstacles (Figure 3B), providing a stabilizing rotational stiffness with respect to the equilibrium nearness function (5).

For a lateral shift away from the tunnel centerline $y \neq 0$ while oriented along centerline $\theta = 0$, the new Fourier series expansion becomes $\mu(\gamma) = \frac{2a}{\pi(a^2-y^2)} + \frac{y}{(a^2-y^2)} \sin\gamma - \sum_{k=2,4,6,\ldots}^{\infty} \frac{4a}{\pi(a^2-y^2)(k^2-1)} \cos k\gamma$. This series contains the equilibrium harmonics $\{A_k : k = 0, 2, 4, \ldots\}$ from (5) with slightly larger amplitudes (when $y \neq 0$), but also contains the fundamental sine harmonic B_1. Hence, outputs that are functions of B_1 will be responsive to the optic flow imbalance due to the lateral shift from the centerline of the tunnel. For obstacles with higher order spatial structure (Figure 3B), we expect to see higher odd sine harmonics in the nearness function, hence outputs a_n generated by weights $\{F_n(\gamma) = \cos n\gamma : n = 2, 4, \ldots\}$ will be functions of $\{B_k : k = 1, 3, 5, \ldots\}$, hence will be responsive to the imbalance due to a lateral shift along the path between them.

The expansion for the most general case $\theta \neq 0$, $y \neq 0$ is given by $\mu(\gamma) = \frac{2a}{\pi(a^2-y^2)} + \frac{y \sin\theta}{(a^2-y^2)} \cos\gamma + \frac{y\cos\theta}{(a^2-y^2)} \sin\gamma - \sum_{k=2,4,6,\ldots}^{\infty} \frac{4a\cos k\theta}{\pi(a^2-y^2)(k^2-1)} \cos k\gamma - \sum_{k=2,4,6,\ldots}^{\infty} \frac{4a \sin k\theta}{\pi(a^2-y^2)(k^2-1)} \sin k\gamma$. In addition to the larger amplitudes on the equlibrium harmonics from (5) when $y \neq 0$, even sine harmonics $\{B_k : k = 2, 4, 6, \ldots\}$ from the phase shift θ are present, as well as the odd sine harmonic B_1 from the imbalance created from the lateral shift y. The only new term, the fundamental cosine harmonic A_1, is a coupling term due to both a phase shift and lateral position shift from the centerline. As in the previous case with obstacles of higher order spatial structure, we expect higher odd cosine harmonics in the nearness function when this coupling occurs (Figure 3B), hence outputs b_n generated by weights $\{F_n(\gamma) = \sin n\gamma : n = 2, 4, \ldots\}$ will be functions of $\{A_k : k = 1, 3, 5, \ldots\}$, therefore responsive to the coupling of optic flow imbalance due to a lateral shift and a orientation change with respect to the desired forward flight path between the obstacles.

3. μ-SHAPING VIA OUTPUT FEEDBACK

In this section we demonstrate the utility of WFI sensory outputs (3) through coupling with planar flight dynamics via static output feedback ($u = Kz$, $K \in \mathbb{R}^{p\times m}$ constant, $u \in \mathbb{R}^p$). For

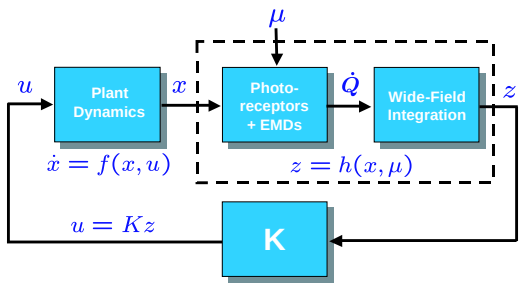

Fig. 4. Closed loop WFI output feedback

analysis and simulation purposes we will use the dynamics of the hovercraft from the Caltech wireless testbed. The vehicle admits planar translational motion (surge, sway) and a single axis of rotary motion (yaw). In the inertial configuration (x, y, θ) the equations of motion $\dot{x} = f(x, u)$ are

$$\begin{aligned} m\ddot{x} &= (F_s + F_p)\cos\theta - b\dot{x} \\ m\ddot{y} &= (F_s + F_p)\sin\theta - b\dot{y} \\ J\ddot{\theta} &= (F_s - F_p)r_o - c\dot{\theta}. \end{aligned} \tag{6}$$

The translational and rotational damping coefficients are denoted by b and c, respectively, the starboard and port thruster forces are denoted by F_s and F_p, and r_o denotes the thruster moment arm. The vehicle mass is given by m and the rotational inertia about the yaw axis is J.

As the goal will be to maintain a forward reference velocity and trajectory along the centerline of the tunnel $(\dot{x}, y, \dot{y}, \theta, \dot{\theta}) = (v_0, 0, 0, 0, 0)$, it will be useful to introduce the following state and

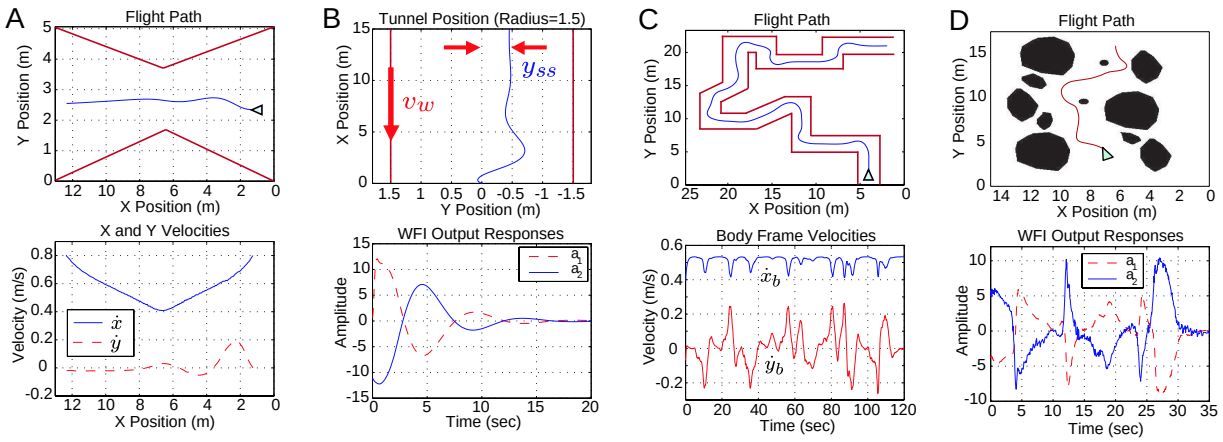

Fig. 5. Simulations of WFI-based navigation. (A) Clutter response for a converging-diverging tunnel (B) Centering response with a moving wall (C) Corridor navigation (D) Obstacle field navigation

input definitions $v = \dot{x}$, $u_1 = F_s + F_p - bv_0$, and $u_2 = F_s - F_p$. Assuming small states (other than v) and control inputs, the linearized equations of motion for a centerline flight trajectory become

$$\begin{aligned} m\dot{v} &= u_1 + b(v_0 - v) \\ m\ddot{y} &= b(v_0\theta - \dot{y}) \\ J\ddot{\theta} &= r_o u_2 - c\dot{\theta} \end{aligned} \tag{7}$$

Table 1 shows the resulting sensory outputs a_0, a_1, b_1 and a_2 in inertial coordinates. The second column is the linearization $z(\boldsymbol{x}) = z(\boldsymbol{x}_0) + \sum_i \frac{\partial z}{\partial x_i}(\boldsymbol{x}_0)\ (x_i - x_{i0})$, with respect to the kinematic variables $\boldsymbol{x} = [\ v\ y\ \dot{y}\ \theta\ \dot{\theta}\ ]'$ along a reference trajectory $\boldsymbol{x}_0 = [\ v_0\ 0\ 0\ 0\ 0\ ]'$, corresponding to a centerline flight path at a constant velocity v_0. Notice in (7) that the v dynamics are decoupled from the y, θ dynamics and in Table 1 the linearized b_1 output is a function of v only and the linearized a_0, a_1, a_2 outputs are functions of $y, \dot{y}, \theta, \dot{\theta}$. Hence, with the linearized system we can effectively decouple the control problem into the *clutter* (forward speed regulation) response and the *centering* response.

Table 1. Inertial WFI Sensory Outputs

WFI Sensory Output	Linearization $z(\boldsymbol{x})$
$a_0 = -\sqrt{2}\dot{\theta} + \frac{y}{\sqrt{2}(a^2-y^2)}\ v$	$-\sqrt{2}\dot{\theta} + \frac{v_0}{\sqrt{2}a^2}y$
$a_1 = \frac{4a}{3\pi(a^2-y^2)}\ (2v\sin\theta - \dot{y}\cos\theta)$	$\frac{4}{3\pi a}\ (2v_0\theta - \dot{y})$
$b_1 = \frac{4a}{3\pi(a^2-y^2)}\ (2v\cos\theta + \dot{y}\sin\theta)$	$\frac{8}{3\pi a}v$
$a_2 = -\frac{y}{2(a^2-y^2)}\ (v\cos 2\theta + \dot{y}\sin 2\theta)$	$-\frac{v_0}{2a^2}y$

For the forward speed regulation task, we define a reference forward velocity r and corresponding scaling factor N and close the loop by setting the thrust input $u_1 = K_{b_1}(Nr - z_{b_1})$. With $r = v_0$, choose $N = 8/(3\pi a)$ for zero steady-state error, and the closed loop dynamics become $\dot{v} = -\frac{1}{m}\left(K_{b_1}N + b\right)(v - v_0)$. One can easily verify that with $K_{b_1} > -b/N$ local stability is achieved.

For the underactuated hovercraft no control input is available in the sideslip (sway) direction. However, the lateral dynamics are coupled to the rotational dynamics through the $bv_0\theta$ term in (7), hence it is possible to accomplish stabilization of both flight modes through the torque input, taken to be $u_2 = K_{a_0}z_{a_0} + K_{a_1}z_{a_1} + K_{a_2}z_{a_2}$. The natural dynamics contain only inertial and viscous terms, therefore to achieve a stable centering/obstacle avoidance response, or equivalently a closed loop where the dynamics are stable with respect to spatial and kinematic perturbations from a balanced nearness function (4), we require $K_{a_1} < 0$ for rotational stiffness and $K_{a_2} > 0$ for lateral stiffness. Additionally, rotational damping can be added with $K_{a_0} > 0$, however this linearized DC component z_{a_0} of $\dot{Q}$ also has an optic flow imbalance term (Table 1), hence we further need the restriction $K_{a_2} > \sqrt{2}K_{a_0}$ to provide the lateral stiffness required for a stable centering response.

It is useful at this point to make some comparisons with experimental assays in tunnel navigation with honeybees, namely the converging-diverging tunnel and the moving wall (Srinivasan *et al.*, 1996). The converging-diverging tunnel investigated the clutter response, as it was observed bees regulated their forward flight speed in proportion to tunnel width; the more narrow the tunnel, the slower the flight speed. In the moving wall experiments, the centering response was examined. Honeybees were directed to fly down a tunnel with one of the walls moving at a constant rate along the flight path. It was observed that when the walls were stationary the bees tended to fly along the centerline, but when one wall was given constant motion along (against) the direction of travel, bees shifted their trajectories toward (away from) the moving wall.

We have constructed simulations based on the full nonlinear planar flight dynamics (6) to qualitatively compare the performance of the WFI

control methodology to these experimental assays. Environments were defined as bitmaps, and the instantaneous optic flow was computed by estimating the depth at the current location and orientation at 60 equidistant circumferential points and combining it with the current kinematics according to (2). WFI outputs are generated by taking the discrete innner product of the instantaneous optic flow with weighting functions corresponding to the body-coordinate observation equations (3). WFI output gains used in the simulation were chosen based on the the performance index of maximizing the bandwidth of the slow (lateral) flight mode in the linearized closed loop system. Figure 5A shows the centering/clutter responses for the hovercraft navigating a converging-diverging tunnel; the forward speed is indeed proportional to tunnel width, as seen in (Srinivasan *et al.*, 1996).

Within the framework we have constructed we can investigate the moving wall assay by modifying the planar tunnel optic flow (1) with a constant left or right wall velocity bias $-v_w\ \hat{\boldsymbol{e}}_x = -v_w \cos\theta\ \hat{\boldsymbol{e}}_{x_b} + v_w \sin\theta\ \hat{\boldsymbol{e}}_{y_b}$. Hence, $\dot{x}_b \mapsto \dot{x}_b + v_w \cos\theta$ and $\dot{y}_b \mapsto \dot{y}_b + v_w \sin\theta$ for $0 \leq \gamma + \theta < \pi$ (left wall movement) or $\pi \leq \gamma + \theta < 2\pi$ (right wall movement). WFI outputs for this case can be computed as in Table 1. For left wall motion, the steady-state value $y = y_{ss}$ along the equilibrium trajectory $x_w : (v = v_0, y = y_{ss}, \dot{y} = 0, \theta = 0, \dot{\theta} = 0)$ that results in a zero torque input $u_2|_{x_w} = 0$ is $y_{ss} = -\frac{a v_w}{2v_0 + v_w}$. Motion opposite the flight direction ($v_w > 0$) will result in a shift right ($y_{ss} < 0$) of the steady-state flight path while motion along the flight direction ($v_w < 0$) will result in a shift left ($y_{ss} > 0$), as observed in (Srinivasan *et al.*, 1996). Also as $v_w \to 0$, $y_{ss} \to 0$ and as $v_w \to \pm\infty$, $y_{ss} \to \mp a$. The simulated hovercraft flight path for left wall motion with $v_w > 0$ is plotted in Figure 5B, along with the time response of the first two spatial cosine harmonics a_1,a_2 of the optic flow. As discussed in the previous section, a_2 provides a corrective torque for the optic flow imbalance, and a_1 provides the opposing rotational stiffness required for stabilization.

The closed loop performance of this output feedback methodology was also evaluated in more complicated environments. Using the same feedback structure and gains, the vehicle was directed to navigate a complicated corridor (Figure 5C) and an obstacle field (Figure 5D). Body velocities are shown for the corridor, and the response of the first two cosine harmonics of the optic flow are shown for the obstacle field. As in Figure 5B, the corrective torque for the optic flow imbalance is supplied by a_2, and the dynamics are stabilized with the opposing rotational stiffness from a_1.

4. CONCLUSIONS

Within the framework presented here, a control-oriented model for spatial wide-field integration (WFI) of retinal image flow was developed. The model provides a unique characterization of information available for feedback from WFI sensory systems, and establishes the connection between global structure of optic flow and the control-relevant information available for feedback.

The analysis presented suggests a more general role for wide-field sensitive neurons in navigation and flight control as well as a novel methodology for utilizing optic flow in bio-inspired applications. Rather than utilizing wide-field sensors as direct estimators of kinematics or depth, it was shown how the spatial harmonics of planar optic flow, extracted with motion-pattern sensitive kernels, correspond to feedback terms which can be used to stabilize the different navigational modes of flight. The proposed WFI output feedback methodology is shown to be equivalent to stabilizing the closed loop dynamics with respect to spatial and kinematic perturbations from a balanced nearness function, and has the advantage of being extremely computationally inexpensive as each required control input can be computed with an inner product of vectors on the order of 60 elements.

Planar flight stabilization and navigation in complicated environments has been demonstrated in simulation, and in addition it is shown that the proposed methodology is sufficient to explain experimentally observed navigational heuristics as the centering and forward speed regulation responses exhibited by honeybees.

REFERENCES

Barrows, G.L., J.S. Chahl and M.V. Srinivasan (2003). Biologically inspired visual sensing and flight control. *The Aeronautical Journal* **107**, 159–168.

Frye, M.A. and M.H. Dickinson (2001). Fly flight: A model for the neural control of complex behavior. *Neuron* **32**, 385–388.

Gibson, J.J. (1950). *The perception of the visual world*. Houghton Mifflin. Boston.

Koenderink, J.J. and A.J. van Doorn (1997). Facts on optic flow. *Biological Cybernetics* **56**, 247–254.

Krapp, H.G. and R. Hengstenberg (1996). Estimation of self-motion by optic flow processing in single visual interneurons. *Letters to Nature* **384**, 463–466.

Srinivasan, M.V., S.W. Zhang, M. Lehrer and T.S. Collet (1996). Honeybee navigation *en route* to the goal: visual flight control and odometry. *J. Exp. Biol.* **199**, 237–244.